Supplementary Information

High anisotropic carrier mobility and strong optical absorption in a biphenylene-like BC_3 monolayer

Shicong Ding,[1,2] Xiaohua Zhang,[2] Jingming Shi,[1] Guochun Yang,[2,a] and Yinwei Li [1,a]

[1]*Jiangsu Key Laboratory of Extreme Multi-Field Materials Physics, School of Physics and Electronic Engineering, Jiangsu Normal University, Xuzhou 221116, China*

[2]*State Key Laboratory of Metastable Materials Science & Technology and Hebei Key Laboratory of Microstructural Material Physics, School of Science, Yanshan University, Qinhuangdao 066004, China*

[a]Authors to whom correspondence should be addressed: yanggc468@nenu.edu.cn and yinwei_li@jsnu.edu.cn

Index·····**Page**

Computational details

An inverse structure design approach guided by band-gap orientation, was performed using the Crystal structure AnaLYsis by Particle Swarm Optimization (CALYPSO) code.[1, 2] This method has been successfully applied to design solar-cell materials and photocatalysts for water splitting.[3, 4] In this work, we carried out a detailed structural search for carbon-rich BC_x (x = 2–6) systems. The target band gap was set to 0.8 eV, and the number of layers was fixed to one. The layer thickness was constrained to 0.2 Å, and a vacuum layer of 20 Å was introduced along the *c*-axis to eliminate interlayer interactions. The initial population consisted of randomly generated structures under specific symmetry constraints, with atomic positions determined by crystallographic symmetry operations. Subsequent local structural optimizations were carried out using the VASP code [5, 6] with the conjugate-gradient algorithm, and the relaxation was considered converged when the total energy change was less than 1×10^{-5} eV per cell. After evaluating the initial generation, 60% of the lowest-enthalpy structures were selected to generate the next generation through the PSO algorithm, while the remaining 40% were randomly regenerated to maintain structural diversity. Structural searches were performed for systems containing 1–4 formula units, with each generation consisting of 40 structures. The evolutionary process was iterated for at least 15 generations to obtain a range of low-energy configurations.

The cohesion energy (E_{coh}) was used to assess structural stability, as defined by:

$$E_{coh} = (E_{BC3} - E_B - 3E_C)/4 \quad (1)$$

Where E_{BC3}, E_B, and E_C represent the energy of the BC_3 monolayer and individual B and C atoms, respectively. In addition, *ab* initio molecular dynamics (AIMD) simulations were performed in the NVT ensemble using a Nosé–Hoover thermostat with SMASS = 0. The simulations were conducted at 300 and 800 K on 4 × 2 × 1 supercells (128 atoms) with Γ-point sampling of the Brillouin zone. A time step of 1 fs was used for a total duration of 6 ps.

Transport calculations were carried out using the AMSET package.[7] Three scattering mechanisms were considered, namely ionized impurity (IMP), acoustic deformation potential (ADP), and polar optical phonon (POP) scattering. The total carrier mobility was obtained according to Matthiessen's rule:[7]

$$1/\mu^{Total} = 1/\mu^{IMP} + 1/\mu^{ADP} + 1/\mu^{POP} \quad (2)$$

The evaluation of IMP, ADP, and POP scattering requires several parameters, including the static dielectric constant, n- and p-type deformation potentials, elastic constants, polar optical phonon frequency, and both static and high-frequency dielectric constants. All these parameters were obtained from first-principles calculations using the VASP code.[5, 6] Specifically, four main steps were followed to compute the parameters required by AMSET.[7] First, uniform non-self-consistent calculations were carried out to generate the electronic inputs for the scattering calculations. Second, the static and high-frequency dielectric constants and the polar optical phonon frequency were

determined using the finite displacement method by setting LEPSILON = True and IBRION = 8. Third, the elastic constants were derived from the stress-strain relationship. Finally, the deformation potentials were calculated through a series of self-consistent calculations, where AMSET automatically generated a set of POSCAR files corresponding to different components of the strain tensor necessary for evaluating the deformation potentials. For the BL-BC_3, HC-BC_3, and BP monolayers, 19 × 13 × 1, 15 × 9 × 1, and 8 × 11 × 1 *k*-point meshes were employed, respectively, for these four independent calculations. The subsequent interpolations were performed using 117 × 53 × 27, 127 × 73 × 33, and 95 × 129 × 21 grids. All calculations were conducted within the framework of the PBE functional, and the band gaps were corrected using a scissor operation based on the HSE06-calculated band gaps.

Supplementary Figures

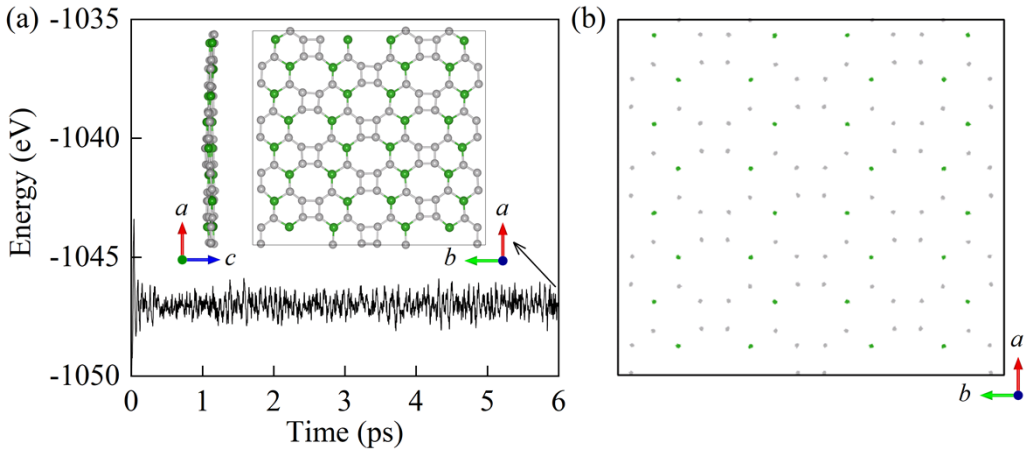

Figure S1. (a) AIMD simulation of BL-BC_3 at 300 K. The inset shows the crystal structure after 6 ps. (b) Corresponding atomic trajectories of B and C atoms within 6 ps. No bond breaking or structural collapse, and atoms exhibit only small vibrations around their lattice sites, confirming the thermal stability of BL-BC_3.

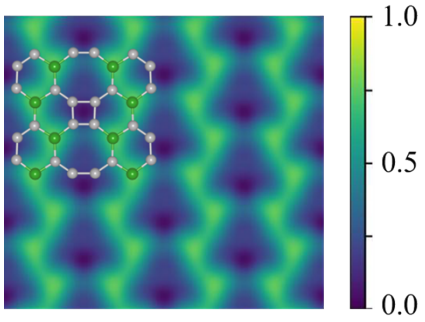

Figure S2. Simulated scanning tunneling microscope (STM) images of the BL-BC_3.

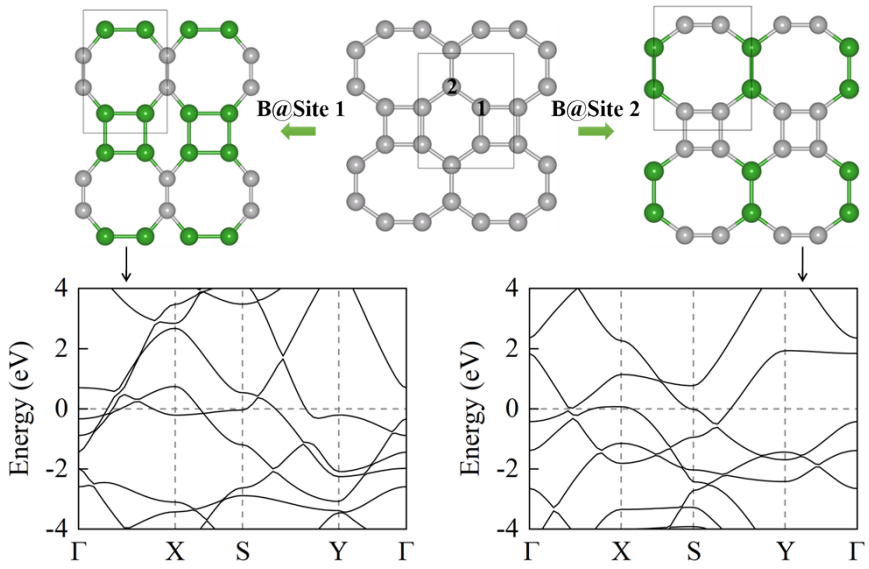

Figure S3. Relaxed structures and corresponding electronic band structures of C_{468} with B substitution at two distinct sites. To investigate the feasibility of tuning C_{468} into a semiconductor, we examined B substitution at two distinct carbon sites. The results indicate that both configurations retain metallic character.

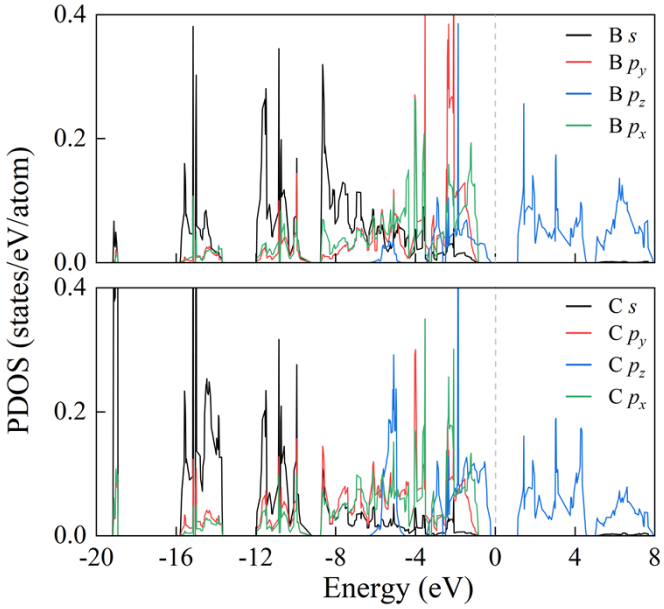

Figure S4. PDOS of BL-BC_3 is plotted over the energy range of –20 eV to 8 eV.

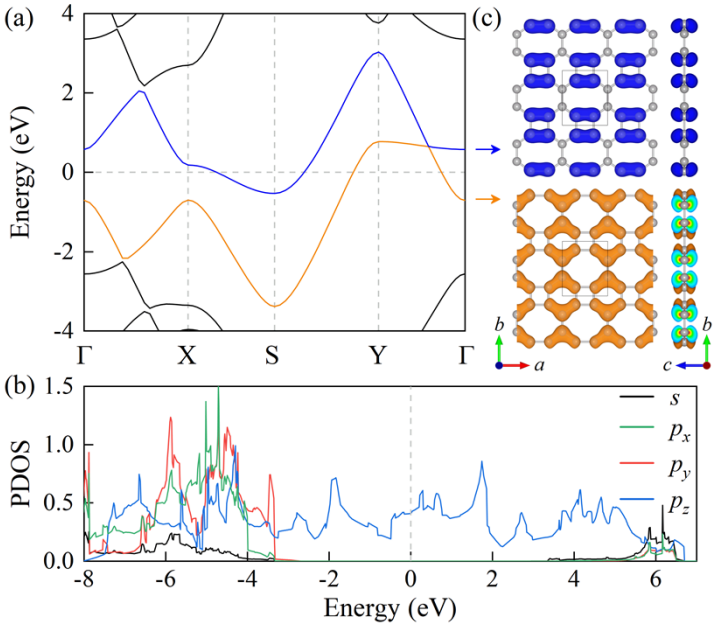

Figure S5. (a) Electronic band structure and (b) projected density of states (PDOS) of C_{468}. (c) Charge density associated with the two bands that cross the Fermi level.

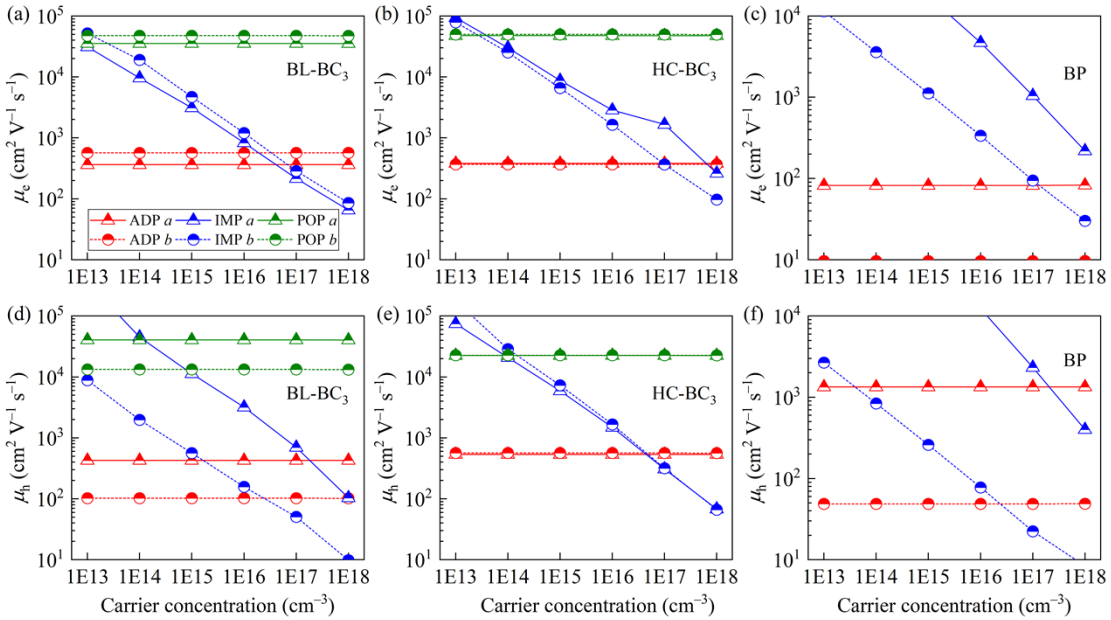

Figure S6. (a)-(c) Electron and (d)-(f) hole mobilities of BL-BC_3, HC-BC_3, and BP monolayers under ADP, IMP, and POP scattering as a function of carrier concentration at 300 K.

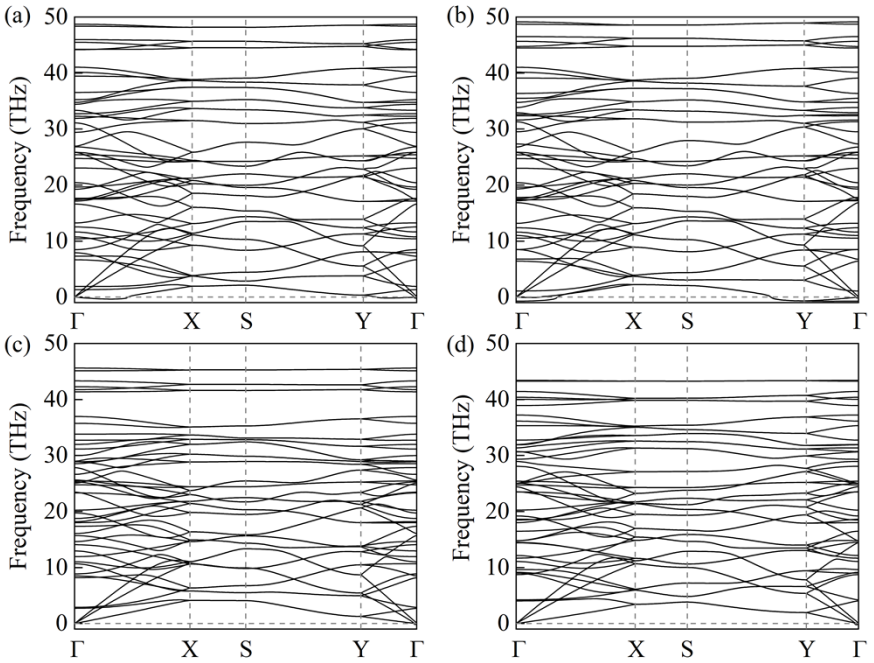

Figure S7. Phonon dispersion curves of the BL-BC_3 monolayer under uniaxial strains of (a) –1% along the *a*-axis, (b) –1% along the *b*-axis, (c) 5% along the *a*-axis, and (d) 5% along the *b*-axis. Only (b) exhibits imaginary frequencies, indicating dynamical instability.

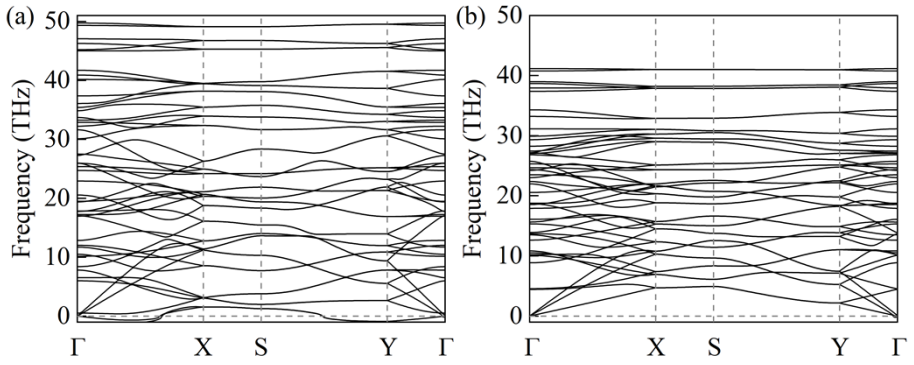

Figure S8. Phonon dispersion curves of the BL-BC_3 monolayer under biaxial strain of (a) –1% and (b) 5%. Dynamical instability is observed under the 1% compression condition.

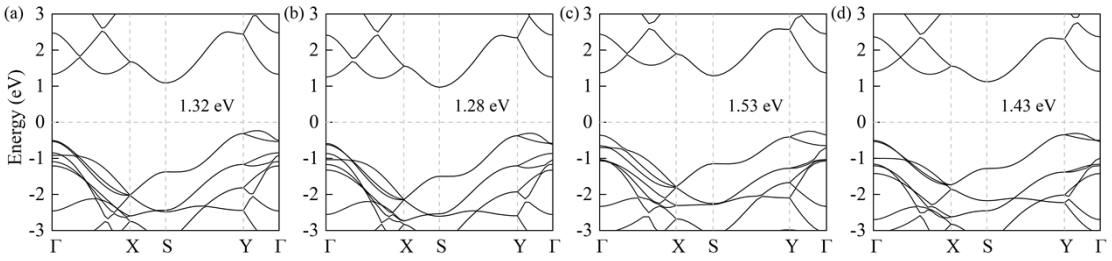

Figure S9. Electronic band structure of the BL-BC_3 monolayer calculated at the HSE06 level under (a) intrinsic conditions, (b) –1% uniaxial strain along the *a*-axis, (c) 5% uniaxial strain along the *a*-axis, and (d) 5% biaxial strain.

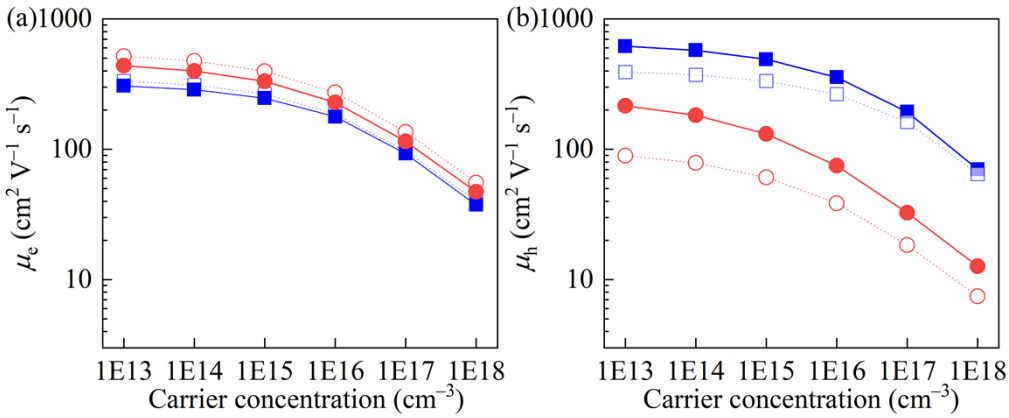

Figure S10. Calculated (a) electron and (b) hole mobilities of the BL-BC_3 monolayer along the *a*-axis (blue) and *b*-axis (red) under –1% uniaxial strain along the *a*-axis. Solid lines represent the strained results, while dashed lines with open symbols denote the intrinsic condition. Results are plotted as a function of carrier concentration at 300 K.

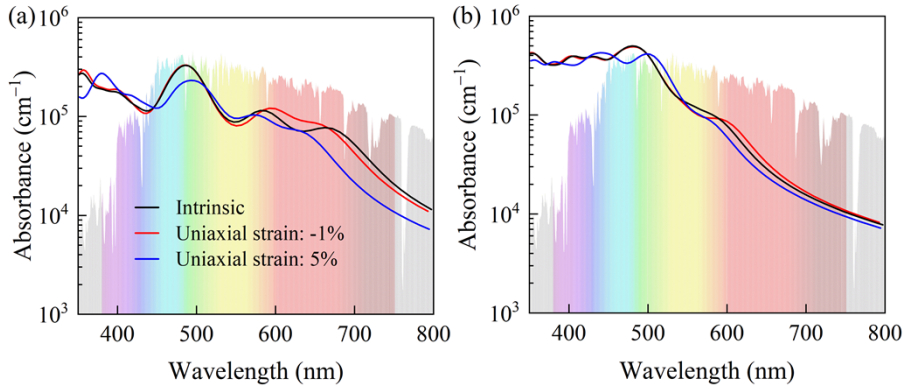

Figure S11. Absorption coefficients of the BL-BC_3 monolayer under uniaxial strain along the *a*-axis calculated using the HSE06 functional. The gray-shaded area denotes the AM1.5 solar spectrum and the visible-light region is highlighted from violet (~ 380 nm) to red (~ 750 nm).

Supplementary Tables

Table S1. Crystal structural parameters of BL-BC_3 monolayer.

Space group	Lattice Parameters	Wyckoff Positions (fractional)			
		Atoms	x	y	z
*Amm*2	a = 20.0000 Å	B (4 *e*)	0.5000	0.3124	-0.3250
	b = 10.3334 Å	C_1 (4 *e*)	0.5000	0.4322	-0.5211
	c = 4.7474 Å	C_2 (4 *e*)	0.5000	0.1833	-0.4985
	α = 90.0000 °	C_3 (4 *e*)	0.5000	0.4268	-0.8339
	β = 90.0000 °				
	γ = 90.0000 °				

Table S2. Parameters used to calculate the scattering rates of the BL-BC_3 monolayer. D^{vb} and D^{cb} are the absolute deformation potentials at the valence and conduction band edge, respectively. ϵ_s and ϵ_∞ are the static and high-frequency dielectric constants in ϵ_0. The effective polar phonon frequency is 36.84 THz.

Parameter	11	12	13	21	22	23	31	32	33
D^{vb}	4.84	0.13	0.02	0.13	13.28	0.02	0.02	0.02	0.01
D^{cb}	11.06	3.03	0.00	3.03	6.91	0.00	0.00	0.00	0.00
ϵ_s	3.06	0.00	0.00	0.00	4.16	0.00	000	0.00	1.12
ϵ_∞	2.89	0.00	0.00	0.00	3.76	0.00	0.00	0.00	1.12

Table S3. Effective masses (m^*/m_0) for holes (m^*_h) and electrons (m^*_e) in intrinsic and strained structures were calculated using the AMSET package.

Monolayer	m^*_h/m_0		m^*_e/m_0	
	a	*b*	*a*	*b*
Intrinsic	0.46	0.51	0.58	0.76
Uniaxial strain (*a*): -1%	0.41	0.67	0.44	0.84
Uniaxial strain (*a*): 5%	0.50	0.39	0.51	0.82
Uniaxial strain (*b*): 5%	0.53	3.41	0.87	0.73
Biaxial strain: 5%	0.50	0.52	0.72	0.79

Table S4. Parameters used to calculate the scattering rates of the BL-BC_3 monolayer under 1% compressive strain along the *a*-axis. D^{vb} and D^{cb} are the absolute deformation potentials at the valence and conduction band edge, respectively. ϵ_s and ϵ_∞ are the static and high-frequency dielectric constants in ϵ_0. The effective polar phonon frequency is 37.52 THz.

Parameter	11	12	13	21	22	23	31	32	33
D^{vb}	5.91	1.13	0.01	1.13	4.56	0.01	0.01	0.01	0.01
D^{cb}	11.11	3.08	0.01	3.08	6.99	0.01	0.01	0.01	0.01
ϵ_s	3.07	0.00	0.00	0.00	4.18	0.00	000	0.00	1.12
ϵ_∞	2.91	0.00	0.00	0.00	3.78	0.00	0.00	0.00	1.12

References

1. Y. Wang, J. Lv, L. Zhu and Y. Ma, *Phys. Rev. B*, 2010, **82**, 094116.
2. Y. Wang, J. Lv, L. Zhu and Y. Ma, *Comput. Phys. Commun.*, 2012, **183**, 2063-2070.
3. R. Xu, H. Zhai, B. Gao and Q. Li, *J. Phys. Chem. Lett.*, 2023, **14**, 4711-4718.
4. R. Xu, H. Zhai, D. Wang, X. Song, D. Zhou and Q. Li, *ACS Mater. Lett.*, 2023, **5**, 2747-2753.
5. G. Kresse and J. Furthmüller, *Phys. Rev. B*, 1996, **54**, 11169-11186.
6. J. P. Perdew, K. Burke and M. Ernzerhof, *Phys. Rev. Lett.*, 1996, **77**, 3865-3868.
7. A. M. Ganose, J. Park, A. Faghaninia, R. Woods-Robinson, K. A. Persson and A. Jain, *Nat. Commun.*, 2021, **12**, 2222.